

## Research Update: Doping ZnO and TiO<sub>2</sub> for solar cells

Robert L. Z. Hoyer, Kevin P. Musselman, and Judith L. MacManus-Driscoll

Citation: [APL Materials](#) **1**, 060701 (2013); doi: 10.1063/1.4833475

View online: <https://doi.org/10.1063/1.4833475>

View Table of Contents: <http://aip.scitation.org/toc/apm/1/6>

Published by the [American Institute of Physics](#)

---

### Articles you may be interested in

[A comprehensive review of ZnO materials and devices](#)

[Journal of Applied Physics](#) **98**, 041301 (2005); 10.1063/1.1992666

[Detailed Balance Limit of Efficiency of p-n Junction Solar Cells](#)

[Journal of Applied Physics](#) **32**, 510 (1961); 10.1063/1.1736034

[Unusual defect physics in CH<sub>3</sub>NH<sub>3</sub>PbI<sub>3</sub> perovskite solar cell absorber](#)

[Applied Physics Letters](#) **104**, 063903 (2014); 10.1063/1.4864778

[Non-equilibrium deposition of phase pure Cu<sub>2</sub>O thin films at reduced growth temperature](#)

[APL Materials](#) **2**, 022105 (2014); 10.1063/1.4865457

[Sodium antimony sulfide \(NaSbS<sub>2</sub>\): Turning an unexpected impurity into a promising, environmentally friendly novel solar absorber material](#)

[APL Materials](#) **4**, 116103 (2016); 10.1063/1.4967206

[Research Update: Strategies for improving the stability of perovskite solar cells](#)

[APL Materials](#) **4**, 091503 (2016); 10.1063/1.4961210

---

PHYSICS TODAY

WHITEPAPERS

#### ADVANCED LIGHT CURE ADHESIVES

Take a closer look at what these environmentally friendly adhesive systems can do

READ NOW

PRESENTED BY  
 **MASTERBOND**  
ADHESIVES | SEALANTS | COATINGS

## Research Update: Doping ZnO and TiO<sub>2</sub> for solar cells

Robert L. Z. Hoyer,<sup>1,a</sup> Kevin P. Musselman,<sup>1,2</sup>  
and Judith L. MacManus-Driscoll<sup>1</sup>

<sup>1</sup>*Department of Materials Science and Metallurgy, University of Cambridge,  
27 Charles Babbage Road, Cambridge CB3 0FS, United Kingdom*

<sup>2</sup>*Department of Physics, University of Cambridge, JJ Thomson Avenue,  
Cambridge CB3 0HE, United Kingdom*

(Received 14 October 2013; accepted 9 November 2013; published online 2 December 2013)

ZnO and TiO<sub>2</sub> are two of the most commonly used n-type metal oxide semiconductors in new generation solar cells due to their abundance, low-cost, and stability. ZnO and TiO<sub>2</sub> can be used as active layers, photoanodes, buffer layers, transparent conducting oxides, hole-blocking layers, and intermediate layers. Doping is essential to tailor the materials properties for each application. The dopants used and their impact in solar cells are reviewed. In addition, the advantages, disadvantages, and commercial potential of the various fabrication methods of these oxides are presented. © 2013 Author(s). All article content, except where otherwise noted, is licensed under a Creative Commons Attribution 3.0 Unported License. [<http://dx.doi.org/10.1063/1.4833475>]

Photovoltaics hold great potential for addressing the world's growing energy demand. The Earth receives 120 000 TW of solar power, whereas the global energy consumption is only 15 TW.<sup>1</sup> Yet photovoltaics contribute only 0.04% of the world's energy production due to the high cost of traditional silicon-based solar cells.<sup>2</sup> To address this issue, it is essential to develop efficient solar cells by using new Earth-abundant, non-toxic, and stable materials, and by implementing low-cost, scalable fabrication methods.<sup>3</sup>

ZnO and TiO<sub>2</sub> are widely used n-type semiconducting materials in new generation solar cells because they are abundant, have high stability, are of simple composition, and therefore amenable to low temperature, low cost, scalable processing methods. These materials tend to be used complementarily in solar cells because they have similarly positioned conduction and valence bands (approximately  $-3.6$  to  $-4.4$  eV below vacuum level for the conduction band and  $-7$  to  $-7.5$  eV for the valence band),<sup>4</sup> but they exhibit different properties that are advantageous for different applications. For example, ZnO tends to have a higher conductivity than TiO<sub>2</sub>, while TiO<sub>2</sub> tends to have a higher chemical stability.<sup>5,6</sup> ZnO can be easily nanostructured,<sup>7</sup> whereas TiO<sub>2</sub> has a much higher dielectric constant and fewer defect states, which leads to less recombination.<sup>8,9</sup> The ability to tune the properties of each oxide in a controlled manner in order to best suit the photovoltaic application and hence maximize the performance of the device is an important challenge. Doping of ZnO and TiO<sub>2</sub> offers an opportunity to achieve this in a cost-effective manner. In this research update, we focus on the recent developments on tuning the properties of these materials through doping and we showcase the most promising methods for fabricating high performance doped materials in a commercially viable way.

The devices covered in this research update are: inorganic solar cells, hybrid solar cells, bulk heterojunction (BHJ) solar cells, dye-sensitized solar cells (DSSCs), and quantum dot solar cells. The operating principles of these devices have been well-covered in the literature, such as Refs. 4 and 10–12.

Doping of ZnO or TiO<sub>2</sub> can tune the built-in potential ( $V_{BI}$ ) and electron-driving force in inorganic, hybrid, and dye-sensitized solar cells by adjusting the conduction band and Fermi level

---

<sup>a</sup>Author to whom correspondence should be addressed. Electronic mail: [rlzh2@cam.ac.uk](mailto:rlzh2@cam.ac.uk). Telephone: +44 1223 767 919.

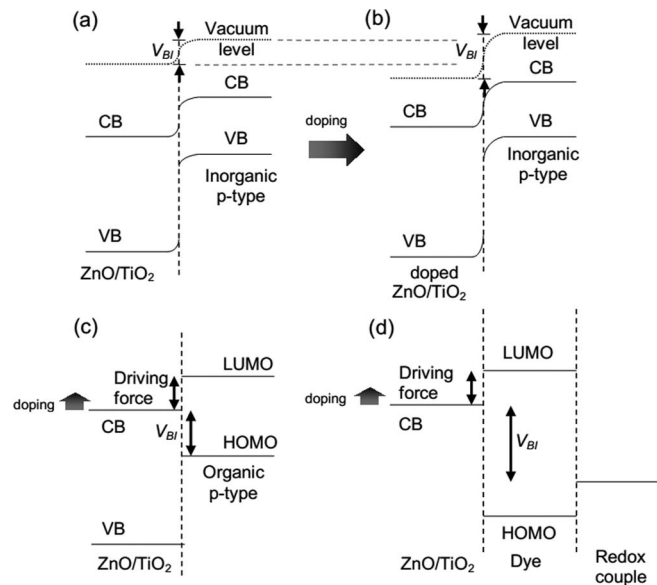


FIG. 1. Band diagrams showing how the tuning of the ZnO/TiO<sub>2</sub> conduction band/Fermi level through doping can influence the built-in potential ( $V_{BI}$ ) of inorganic (a) and (b), organic (c), and dye-sensitized (d) solar cells. The driving forces for electron injection in hybrid and dye-sensitized solar cells are also indicated in (c) and (d), respectively.<sup>14–17</sup>

positions. One of the most common methods of tuning the ZnO conduction band is through Mg doping. This occurs because the Mg 3s orbitals hybridize and raise the energy level of the Zn 4s orbitals in the ZnO conduction band minimum, leading to an increased bandgap.<sup>13</sup>

Recently, Zn<sub>1-x</sub>Mg<sub>x</sub>O has been employed to increase the efficiency ( $PCE$ ) of ZnO–Cu<sub>2</sub>O solar cells. As shown in Figs. 1(a) and 1(b) and Table I, when the Fermi level of the doped ZnO is increased through a raised conduction band, the increased band bending leads to an increased  $V_{BI}$ , resulting in an increased open-circuit voltage ( $V_{OC}$ ).<sup>18</sup> On the other hand, microstructure can be compromised by doping. Duan *et al.* found that when the Mg content of the metal-organic chemical vapor deposited (MOCVD) Zn<sub>1-x</sub>Mg<sub>x</sub>O was above 10%, the MOCVD films were too rough for the p-type Cu<sub>2</sub>O layer to be electrodeposited on top.<sup>18</sup> Olson *et al.* found a similar film roughening when depositing Zn<sub>1-x</sub>Mg<sub>x</sub>O by sol-gel. But in their case, the increased roughness was fortuitous because the spin-coated polymer absorber they used (poly(3-hexylthiophene-2,5-diyl) or P3HT) remained adherent to the Zn<sub>1-x</sub>Mg<sub>x</sub>O films and the increased roughness raised the current extracted for their hybrid devices (Fig. 1(c)) by increasing the interfacial area.<sup>15</sup> Doping can also be detrimental to carrier mobility, and Mg-doping has been found to decrease the mobility of ZnO by increasing the effective electron mass owing to the change in the band structure.<sup>19</sup> This limits the amount of Mg-doping for improving device performance.

Smoother Zn<sub>1-x</sub>Mg<sub>x</sub>O films have been deposited for solar cells using atomic layer deposition (ALD), where root-mean-square roughness values of a few nanometers were obtained.<sup>20</sup> But unlike sol-gel deposition, ALD (like MOCVD) is limited because of the need for vacuum-processing, which restricts the size of the substrates, increases the total deposition time, and increases the processing complexity and cost.<sup>18,21,22</sup> Also, organometallic precursors, which are often expensive and pyrophoric, are typically used in MOCVD or ALD.<sup>22</sup> Sol-gel is advantageous over these two techniques because it involves air-processing using non-pyrophoric precursors, in addition to providing greater flexibility in producing films with new compositions due to the simplicity of the process. As such, a wide variety of novel dopants have been introduced to ZnO or TiO<sub>2</sub> using sol-gel deposition. The disadvantage is that only one substrate can be processed at a time if spin-coating is used for depositing the film from the sol, and the precursors and products often require ageing at temperatures of up to 600 °C.<sup>22</sup> ALD films are advantageous over sol-gel and MOCVD films (which require ~520 °C processing)<sup>18</sup> because relatively low temperatures of only ~120–150 °C are required.<sup>23</sup>

TABLE I. Comparison of the fabrication methods and performance parameters of the highest efficiency solar cells using doped ZnO/TiO<sub>2</sub> with the equivalent undoped ZnO/TiO<sub>2</sub>. N.B.: FTO is fluorine-doped tin oxide and ITO is indium-doped tin oxide.

Dopant	Fabrication	Cell architecture		$J_{SC}$ (mA cm <sup>-2</sup> )	$V_{OC}$ (V)	$FF$ (%)	$PCE$ (%)	Ref.
ZnO								
Mg	MOCVD	Glass/FTO/	Doped ( $x = 0.10$ )	3.00	0.575	42	0.71	18
		Zn <sub>1-x</sub> Mg <sub>x</sub> O/Cu <sub>2</sub> O/Ag	Undoped	2.38	0.251	34	0.21	
Mg	Sol-gel	Glass/ITO/Zn <sub>1-x</sub> Mg <sub>x</sub> O/	Doped ( $x = 0.25$ )	0.33	0.83	42	0.12	15
		P3HT/Ag	Undoped	0.26	0.5	50	0.065	
Mg	Sol-gel	Glass/FTO/ Zn <sub>1-x</sub> Mg <sub>x</sub> O/	Doped ( $x = 0.05$ )	9.98	0.71	58	4.11	24,27
		N719/I <sup>-</sup> , I <sub>3</sub> <sup>-</sup> /Pt/FTO/glass <sup>a</sup>	Undoped	6.15	0.67	47	1.97	
TiO <sub>2</sub>								
Mg	Solvothermal	Glass/FTO/Ti <sub>1-x</sub> Mg <sub>x</sub> O <sub>2</sub> /SFD-5/electrolyte/Pt/FTO/glass <sup>b</sup>	Doped (Br <sub>3</sub> <sup>-</sup> , Br <sup>-</sup> )	1.80	1.21	55	1.2	16
			Doped (I <sub>3</sub> <sup>-</sup> /I <sup>-</sup> )	2.17	0.67	51	0.74	
			Undoped (I <sub>3</sub> <sup>-</sup> /I <sup>-</sup> )	2.73	0.55	48	0.72	
Sb	Sol-gel	Glass/FTO/ Ti <sub>1-x</sub> Sb <sub>x</sub> O /PbS/Au/Ag	Doped	17.2	0.52	54	4.74	26
			Undoped	11.3	0.56	59	3.66	
Zr	Sol-gel	Glass/FTO/Ti <sub>1-x</sub> Zr <sub>x</sub> O /PbS/Au/Ag	Doped	17.0	0.56	61	5.69	26
			Undoped	11.3	0.56	59	3.66	

<sup>a</sup>N719 is *cis-bis* (isothiocyanato) *bis*(2,20-bipyridyl-4,40-dicarboxylato)-ruthenium(II)-*bis*-tetrabutylammonium or RuC<sub>58</sub>H<sub>86</sub>N<sub>8</sub>O<sub>8</sub>S<sub>2</sub>,<sup>27</sup> which is reported to have an effective bandgap of 1.60 eV.<sup>28</sup>

<sup>b</sup>SFD-5 in Ref. 16 is a 2.66 eV bandgap triethoxysilyl-coumarin dye.

DSSCs based on ZnO photoanodes have not been found to be as efficient as ones with TiO<sub>2</sub>, partially due to recombination that arises as a result of the instability of ZnO in contact with acidic dyes (e.g., the common N719 dye) and the formation of Zn<sup>2+</sup>-dye aggregates.<sup>24</sup> Through the substitutional replacement of Zn<sup>2+</sup> with Mg<sup>2+</sup> both of these factors were alleviated. Additionally, raising the conduction band increased the  $V_{BI}$  by increasing the conduction band-redox potential offset, leading to an increased  $V_{OC}$ . However, when the Mg content was too high, the Mg<sup>2+</sup> occupying interstitial sites was thought to create shallow acceptor levels above the Fermi level, leading to increased recombination. Hence, doping led to improved stability, increased  $V_{OC}$  and reduced charge recombination at low doping levels, and high charge recombination at high doping levels. A Mg content of 5 mol.% represents the best compromise between these factors (Table I).<sup>24</sup>

Doping TiO<sub>2</sub> with Mg has also been found to raise the conduction band. This was attributed to the formation of Mg-Ti mixed oxides, since MgTiO<sub>3</sub> and MgTi<sub>2</sub>O<sub>5</sub> have larger bandgaps than undoped TiO<sub>2</sub>.<sup>16,25</sup> The raised conduction band resulted in an increased  $V_{BI}$  and  $V_{OC}$  for DSSCs (Fig. 1(d)). These were further increased by changing the commonly used I<sub>3</sub><sup>-</sup>, I<sup>-</sup> redox couple with Br<sub>3</sub><sup>-</sup>, Br<sup>-</sup> which has a lower redox couple potential, along with surface treatment of the doped TiO<sub>2</sub> electrodes using MgO and ethanoic acid to reduce back-electron transfer. As a result an extremely high  $V_{OC}$  of 1.2 V was obtained (Table I).<sup>16</sup>

Reducing the bandgap of TiO<sub>2</sub> through doping has also been undertaken to improve the alignment of the TiO<sub>2</sub> with the conduction band of infrared-absorbing PbS quantum dots (QDs). As illustrated in Fig. 2, Liu *et al.* found that the conduction band of sol-gel deposited undoped TiO<sub>2</sub> was slightly above that of the QDs (Fig. 2(a)) and limited electron injection. Doping the TiO<sub>2</sub> with Zr or Sb lowered the TiO<sub>2</sub> conduction band (Figs. 2(b) and 2(c)). Having the QD conduction band exactly aligned with the TiO<sub>2</sub> conduction band (as in the case of the Zr:TiO<sub>2</sub> in Fig. 2(b)) was found to produce the most efficient devices because when the TiO<sub>2</sub> conduction band was too low (as with Sb:TiO<sub>2</sub>), the  $V_{OC}$  was reduced by a lower quasi-Fermi level offset between the TiO<sub>2</sub> and QDs (lower  $V_{BI}$ , see Figs. 1(a) and 1(b)), and possibly in addition to electron thermalization down the metal oxide

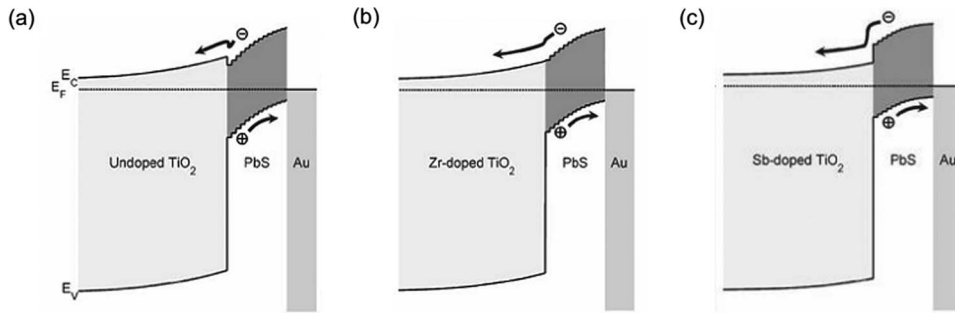


FIG. 2. Band alignment of (a) undoped  $\text{TiO}_2$ , (b) Zr-doped  $\text{TiO}_2$ , and (c) Sb-doped  $\text{TiO}_2$  with 1.1 eV  $E_g$  PbS quantum dots. Reproduced by permission from H. Liu, J. Tang, I. J. Kramer, R. Debnath, G. I. Koleilat, X. Wang, A. Fisher, R. Li, L. Brzozowski, L. Levina, and E. H. Sargent, *Adv. Mater.* **23**, 3832 (2011). Copyright 2011 Wiley-VCH.

TABLE II. Comparison of the effect of doping of  $\text{TiO}_2$  to improve visible light absorption on the performance of DSSCs.

Dopant	Fabrication	Cell architecture		$J_{SC}$ ( $\text{mA cm}^{-2}$ )	$V_{OC}$ (V)	$FF$ (%)	$PCE$ (%)	Ref.
$\text{TiO}_2$								
N	Thermal	Glass/FTO/ $\text{TiO}_2$ :N/	Doped	17.9	0.69	62	8	30
		N719/ $\text{I}_3^-$ , $\text{I}^-$ /Pt/FTO/glass	Undoped	13.3	0.685	66	6	
S	Ball milling	Glass/FTO/ $\text{TiO}_2$ :S/	Doped	14.6	0.659	68.2	6.91	31
		N719/ $\text{I}_3^-$ , $\text{I}^-$ /Pt/FTO/glass	Undoped	11.2	0.688	68.5	5.56	
Cr	Sol-gel	FTO/ $\text{TiO}_2$ /Cr: $\text{TiO}_2$ /	Doped (10 at%)	15.2	0.78	71	8.4	32
		N719/ $\text{I}_3^-$ , $\text{I}^-$ /Pt	Undoped	13.0	0.79	69	7.1	

conduction band tail.<sup>12,26</sup> Optimizing the band alignment (balancing  $V_{OC}$  and short-circuit current density,  $J_{SC}$ ) through conduction band tuning is therefore essential for maximizing efficiency.

Although using  $\text{TiO}_2$  photoanodes has produced the most efficient DSSCs,<sup>24</sup> the  $\text{TiO}_2$  needs to be sensitized with a dye because the  $\text{TiO}_2$  bandgap is too wide to absorb visible light.<sup>29</sup> If this bandgap could be reduced the photocurrent generated could be increased. N-doping of  $\text{TiO}_2$  improves visible light absorption of dye-sensitized  $\text{TiO}_2$  (Fig. 3(a)) by introducing new states close to the valence band.<sup>30</sup> As a result, additional photocurrent is generated in the devices, while the  $V_{OC}$  is not sacrificed, since the conduction band is not shifted (Table II).<sup>30</sup> Ball-milling  $\text{TiO}_2$  with thiourea is a low temperature method for S-doping  $\text{TiO}_2$ , which also improves the visible light absorption and therefore the  $J_{SC}$  when used in DSSCs (Table II). However, XPS measurements showed that  $\text{S}^{6+}$  substitution of  $\text{Ti}^{4+}$  rather than  $\text{S}^{2-}$  substitution of  $\text{O}^{2-}$  occurred, meaning that the conduction band was affected and the  $V_{OC}$  was reduced with doping.<sup>31</sup> Sol-gel Cr-doped  $\text{TiO}_2$  has also been found to reduce the bandgap and enhance visible light absorption. More remarkably, incorporating 10 at.% Cr also made the  $\text{TiO}_2$  p-type. By inserting this p-type layer between n-type undoped  $\text{TiO}_2$  and the dye (Fig. 3(b)), back-recombination was reduced and fill factors ( $FF$ s) increased.<sup>32</sup>

Injected electrons can tunnel through the p-n junction of a solar cell via trap states at the interface and recombine with a hole in the p-type material, as illustrated in Fig. 4(a). This lowers the efficiency of solar cells by reducing the  $V_{OC}$  and  $FF$ , and can be prevented by inserting a buffer layer at the interface (Fig. 4(b)). Unlike  $\text{TiO}_2$ , undoped ZnO tends to have too many defect states and a carrier concentration that is too high to be a buffer layer. This can be controlled through doping. Vacuum sputtered Mg-doped ZnO has been used in SnS solar cells and this increased the efficiency from 0.29% to 1.10% (Table III) because the built-in potential at the interface increased with the ZnO Fermi level, resulting in a stronger driving force to prevent recombination.<sup>33</sup> More effective ZnO buffer layers were produced by doping amorphous ZnO with tin (a-ZTO). This lowered the

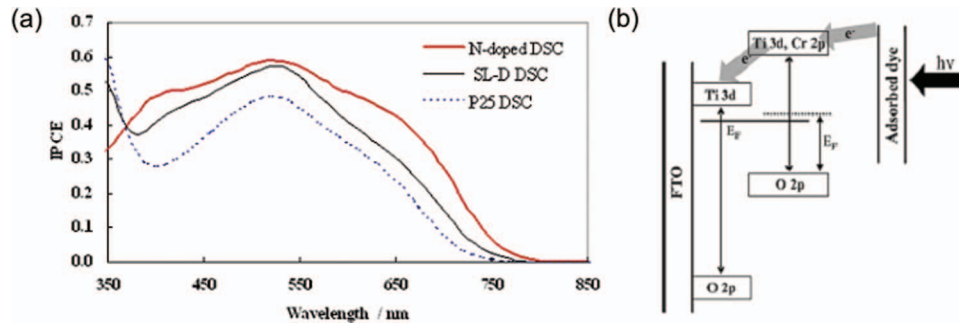


FIG. 3. (a) IPCE (incident photon-to-current efficiency) of DSSCs showing that N719 dye sensitized onto N-doped  $\text{TiO}_2$  had improved IPCE compared to undoped  $\text{TiO}_2$  (SL-D and P25). Reprinted with permission from T. Ma, M. Akiyama, E. Abe, and I. Imai, *Nano Lett.* **5**, 2543 (2005). Copyright 2005 American Chemical Society. (b) Schematic showing the cascade of energy levels from the dye LUMO to the conduction bands of the Cr: $\text{TiO}_2$  and undoped  $\text{TiO}_2$ . Reproduced by permission from C. Kim, K.-S. Kim, H. Y. Kim, and Y. S. Han, *J. Mater. Chem.* **18**, 5809 (2008). Copyright 2008 from Royal Society of Chemistry.

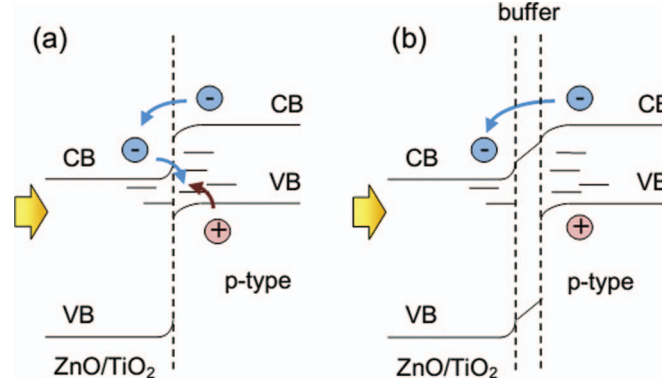


FIG. 4. Illustration of (a) back recombination via interfacial trap states without a buffer layer and (b) prevention of back recombination by inserting a defect-free buffer layer.<sup>35</sup>

TABLE III. Comparison of doped ZnO used as buffer layers at the heterointerface to reduce recombination

Dopant	Fabrication	Cell architecture		$J_{SC}$ ( $\text{mA cm}^{-2}$ )	$V_{OC}$ (V)	$FF$ (%)	$PCE$ (%)	Ref.
Mg	Sputtering	Glass/ITO/ $\text{Zn}_{1-x}\text{Mg}_x\text{O}/\text{SnS}/\text{Cu}$	Doped ( $x = 0.18$ )	13.3	0.23	36	1.10	33
			Undoped	10.9	0.10	27	0.29	
Sn	ALD	Fused silica/Ti/Au/ $\text{Cu}_2\text{O}/\text{Zn}_{1-x}\text{Sn}_x\text{O}/\text{AZO}/\text{Al}$	Doped ( $x = 0.21$ )	7.37	0.553	65	2.65	3
			Undoped	7.26	0.462	61.8	2.07	
N	AALD	Glass/ITO/ $\text{ZnO:N}/\text{PbS}/\text{MoO}_3/\text{Au}$	Doped	10.5	0.46	...	1.5	35
			Undoped	10.5	0.27	...	0.8	

density of defect states, raised the ZnO Fermi level, and reduced the carrier concentration from  $1.8 \times 10^{19} \text{ cm}^{-3}$  (undoped) down to below  $3.5 \times 10^{16} \text{ cm}^{-3}$  (21 at.% Sn). All of these factors served to reduce back-recombination in  $\text{Cu}_2\text{O}$ -a-ZTO-Al:ZnO solar cells and increased the efficiency to a record value of 2.65% (Table III). ALD was used to deposit the a-ZTO because a thin (5 nm) film was needed to allow current to pass through the buffer layer.<sup>3</sup> However, ALD is a vacuum-based technique, and a more scalable alternative is atmospheric ALD (AALD).<sup>22,34,35</sup> The key feature is a gas manifold, in which the metal precursor and oxidant are spatially separated by inert nitrogen gas channels, which allows the films to be deposited in open-atmosphere, at a rate of approximately

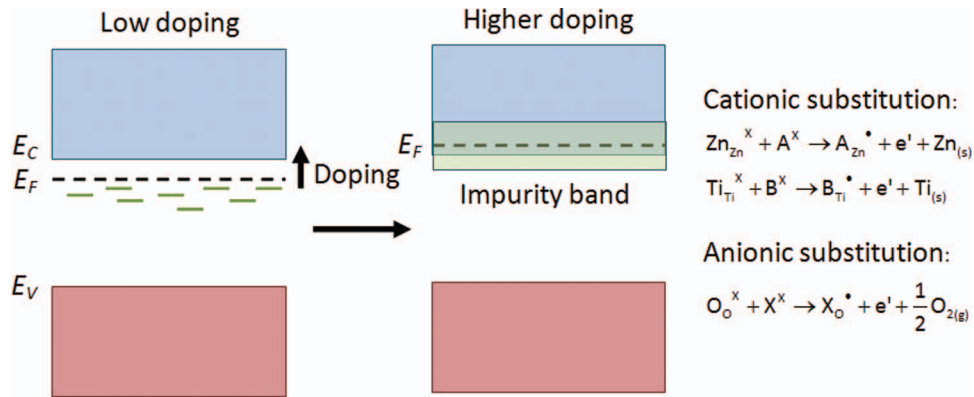


FIG. 5. Illustration of how doping a semiconductor to increase its carrier concentration can make it degenerate and highly conductive.  $E_C$  is the conduction band minimum,  $E_F$  the Fermi level, and  $E_V$  the valence band maximum. Example doping reactions that would increase the carrier concentration of ZnO or TiO<sub>2</sub> are shown in Kröger Vink notation, where the body denotes the species, subscript the lattice position (e.g., Zn = Zn lattice sites), and superscript the charge ( $X$  = no charge overall in the lattice, dot = positive charge, comma = negative charge). In the example reactions, A and B are cations with valencies of three and four, respectively. X is an anion with a valency of one. Since these ions have valencies one more (cations) or less (anion) than the ion they are replacing, they have one extra positive charge compared with the host ions and donate an extra electron to the lattice.<sup>36</sup>

one order of magnitude higher than conventional ALD.<sup>22,34</sup> AALD has been used to incorporate 0.22 at.% N into ZnO to reduce the ZnO carrier concentration and therefore to reduce interfacial recombination in PbS colloidal quantum solar cells (CQDSCs).<sup>35</sup>

Doping ZnO or TiO<sub>2</sub> to increase the carrier concentration can lead to transparent conducting oxides (TCOs) based on ZnO and TiO<sub>2</sub>, or layers to improve current extraction from solar cells. Typically, these dopants substitute lattice ions. Cationic substituents must have a higher valency than the host cation, and anionic substituents must have a lower valency than the host anion in order to introduce extra charge carriers. This is illustrated by the substituent doping reactions shown in Fig. 5. Often, shallow donor states are created by the introduction of these dopants, which form an impurity band. When the impurity band overlaps with the bottom of the conduction band and the Fermi level rises to within the conduction band (due to the increased carrier concentration), the semiconductor becomes degenerate and conducts like a metal, thus giving rise to TCOs.<sup>36</sup>

Transparent conducting oxides (TCOs) are essential for admitting light and collecting charge in solar cells. But the common TCOs (fluorine-doped tin oxide or FTO, and indium-doped tin oxide or ITO) are either limited in conductivity (FTO) or are expensive (ITO).<sup>36,37</sup> Al-doped ZnO (AZO) and Ga-doped ZnO (GZO) are both more abundant than In, less expensive and non-toxic, and more conductive than FTO.<sup>36,38</sup> AZO has been deposited by vacuum-based methods, such as pulsed laser deposition (PLD), sputtering, and ALD.<sup>39,40</sup> Low pressure chemical vapor deposition (LP-CVD) has been used to deposit rougher AZO films, which scatters light to improve absorption in the solar cells (i.e., the films have a higher haze factor), leading to higher  $J_{SC}$ s in amorphous silicon solar cells (Table IV).<sup>41</sup> However, AZO has limited thermal stability and longevity due to the high reactivity of Al.<sup>42</sup> Ga-doped ZnO is more stable, conductive, and transparent than AZO.<sup>37</sup> In P3HT:PCBM ([6,6]-phenyl-C61-butyric acid methyl ester) devices, the efficiencies of devices with GZO as the TCO were comparable to using ITO (Table IV).<sup>37</sup> GZO is also less resistive and more transparent than FTO, but is susceptible to acid etching, which limits the use of GZO in DSSCs, where the dye is acidic. This was overcome by protecting the GZO with a thin TiO<sub>2</sub> layer (Table IV).<sup>43</sup>

Nb-doping is a common method of producing TCOs based on anatase TiO<sub>2</sub>. Both Nb and Ti are more abundant than In.<sup>44</sup> Resistivities as low as  $(2-3) \times 10^{-4} \Omega \text{ cm}$  (with 6% Nb) and visible light transmittance >97% have been obtained, but these results were achieved using high-temperature processes, such as PLD and sputtering.<sup>44</sup> Nb:TiO<sub>2</sub> has been employed in lieu of pure TiO<sub>2</sub> as a more conductive protective layer for ZnO-based TCOs in DSSCs. As seen in Table IV, AZO coated with PLD Nb:TiO<sub>2</sub> improved the efficiency of DSSCs compared with using only AZO as the TCO.<sup>45</sup>

TABLE IV. Comparison of the key properties of transparent conducting oxides (TCOs) made from doped ZnO or TiO<sub>2</sub> and the performance of the devices based on these TCOs. N.B.: In this table, all values in the resistivity column are resistivity values, apart from where sheet resistance values are given. N.B.B.: The transmittance values reported pertain to the visible light (400–800 nm) transmittance.

Dopant	Fabrication	Cell architecture		$\rho \times 10^{-3}$ ( $\Omega$ cm)	Transmittance (%)	$J_{SC}$ (mA cm <sup>-2</sup> )	PCE (%)	Ref.
ZnO								
Al	LP-CVD	Glass/Al:ZnO	Al:ZnO	...	~83	16.04	7.77	41
		or ZnO or FTO/	ZnO	...	~85	10.26	3.08	
		p-i-n a-Si:H/Al	FTO	...		14.35	7.61	
Ga	Ion-beam	Glass/Ga:ZnO or ITO/ZnO/	Ga:ZnO/ZnO	...	~80	11.64	3.40	37
		P3HT:PCBM/MoO <sub>3</sub> /Au <sup>a</sup>	ITO/ZnO	...	~80	12.05	3.54	
Ga	PLD	Glass/Ga:ZnO/TiO <sub>2</sub> /	Ga:ZnO	6.87 $\Omega$ /sq	~85	9.01	3.96	43
TiO <sub>2</sub>								
Al (ZnO)	Sputtering (AZO)	Fused silica/Al: ZnO/Nb:TiO <sub>2</sub> /TiO <sub>2</sub>	AZO/Nb:TiO <sub>2</sub>	0.38	~70	8.52	3.8	45
Nb (TiO <sub>2</sub> )	PLD (Nb:TiO <sub>2</sub> )	NP/N719/I <sub>3</sub> <sup>-</sup> , I <sup>-</sup> /Pt/FTO/glass	AZO only	68	~80	4.66	1.9	

<sup>a</sup>PCBM is [6,6]-phenyl-C61-butyric acid methyl ester, PEDOT:PSS is poly(3,4-ethylenedioxythiophene):poly(styrenesulfonate).<sup>47</sup>

Attempts have been made to deposit Nb:TiO<sub>2</sub> in low-temperature ambient conditions using sol-gel deposition, but it was found that the films were not highly conductive unless they were annealed at high temperatures.<sup>46</sup> It is therefore challenging to produce Nb:TiO<sub>2</sub> using an easily-scalable ambient method.

Doping of ZnO or TiO<sub>2</sub> to improve the conductivity can also be used to increase the photocurrent in solar cells by reducing the series resistance. One application is blocking layers in bulk heterojunction solar cells (BHJs). BHJs are organic solar cells in which the electron-donating and electron-accepting polymers are intimately mixed together to maximize the interfacial area for charge separation.<sup>11,22</sup> Since both phases are in contact with each electrode, blocking layers are needed to prevent recombination at the electrodes.<sup>22,34</sup> This is illustrated in Fig. 6. ZnO and TiO<sub>2</sub> are common hole blocking layer (HBL) materials because they have high electron mobilities but low hole mobilities and large ionization energies that inhibit hole transfer.<sup>22,34</sup> Sol-gel In-doping of ZnO has been found to reduce the sheet resistance from 42.3 to 35  $\Omega$  cm and increased the transparency to visible light, resulting in an increased device efficiency due to an increased photocurrent (Table V).<sup>48</sup> A similar result was obtained by LiF doping of ZnO. This is because Li occupies the interstitial sites and dissociates to give Li<sup>+</sup>, and the F component occupies substitutional O<sup>2-</sup> sites where it accepts one fewer electron than O<sup>2-</sup>, both of which lead to an increased carrier concentration (Table V).<sup>49</sup> LiF:ZnO has been shown to have a transmittance >95% for visible light,<sup>49</sup> and is not as rare or toxic as In, making LiF doping advantageous over In-doping.<sup>50</sup>

Nb:ZnO nanoparticles synthesized using flame-spray pyrolysis have also been used in a novel way in BHJs: they were incorporated into the P3HT:PCBM blend to form an organic-inorganic composite. Nb-doping reduced the sizes of the nanoparticles, which then scatter more light and leads to an increased light absorption in the blend, thus maximizing the incident photon-to-current efficiency (IPCE) and  $J_{SC}$ . Furthermore, the P3HT (absorber), PCBM, and Nb:ZnO nanoparticles present a cascade in upper energy levels (LUMO/conduction band), which aids electron transfer from the P3HT to PCBM to the Nb:ZnO. Since the Nb:ZnO has its conduction band approximately aligned with the Al top contact Fermi level, the cascading energy levels improve charge extraction and increase the efficiency through an increased  $J_{SC}$  (Table V).<sup>51</sup>

DSSCs with ZnO photoanodes can have improved efficiency through more conductive photoanodes (through F doping via chemical bath deposition).<sup>52</sup> Doping TiO<sub>2</sub> photoanodes with either F or

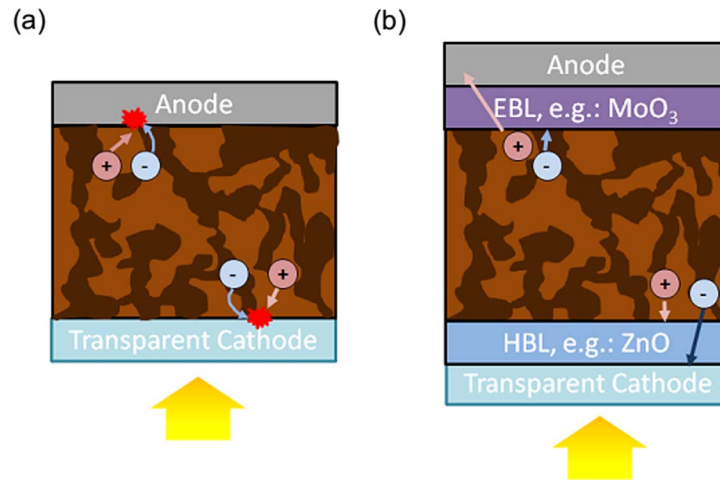


FIG. 6. Illustration showing (a) BHJ without blocking layers, and (b) BHJ with blocking layers.

B can also improve the conductivity, leading to an increase in the efficiency through a  $J_{SC}$  increase (B dopants are reported to increase the carrier concentration of  $\text{TiO}_2$  by favoring the formation of oxygen vacancies).<sup>6,53</sup> A similar effect was also observed through Zn-doping the  $\text{TiO}_2$ , which is thought to improve the electron transport properties, although the specific mechanisms involved in carrier generation have not been thoroughly studied.<sup>54</sup> Excessive doping, however, was found to introduce surface oxygen vacancies, which acted as recombination centers.<sup>54</sup>  $\text{Ta}^{5+}$  and  $\text{Nb}^{5+}$  have also successfully increased the conductivity of  $\text{TiO}_2$  photoanodes in DSSCs. However, it was found that the increase in carrier concentration led to an increase in the flat-band potential. This increases the driving force for electron injection (contributing to the  $J_{SC}$  increase), but decreases the offset from the redox couple potential resulting in a decrease in the  $V_{OC}$ .<sup>55,56</sup>

The advantages of stability and conductivity offered by  $\text{Nb}:\text{TiO}_2$  have also been used to improve the performance of hybrid solar cells with MEH-PPV as the absorbing p-type polymer. As can be seen in Table V, the improved conductivity almost tripled the  $J_{SC}$ , leading to the efficiency almost doubling.<sup>57</sup> The other doping methods to improve the conductivity of  $\text{TiO}_2$  or  $\text{ZnO}$  could also be applied to obtain a similar improvement in performance of hybrid solar cells.

In summary, we have described how different dopants and the methods for including them in  $\text{ZnO}$  and  $\text{TiO}_2$  have their advantages and disadvantages. To optimize solar cell performance, it is critical to fine tune the conductivity to balance the increased photocurrent with increased recombination or decreased  $V_{OC}$ .

From this research update, it can be seen that for each case of  $\text{ZnO}$  and  $\text{TiO}_2$  used in solar cells, there are a variety of dopants available to tailor the properties and optimize the device performance. However, some dopants stand out as being more effective. In some applications, certain dopants have been extremely widely used, even though some disadvantages associated with those dopants have not yet been overcome. One such example is Mg-doping of  $\text{ZnO}$ . While it is possible to dope  $\text{ZnO}$  with Mg over an extremely wide range for a variety of applications, doping reduces the mobilities. Other dopants that increase the bandgap, while minimizing the reduction in mobility should be explored.

Ga-doped  $\text{ZnO}$  should be studied in the future more than Al-doped  $\text{ZnO}$ , since GZO is more conductive, transparent, and stable than AZO.<sup>36,42,62</sup> Producing rougher TCOs to increase the haze factor and light absorption should also be investigated. However, TCOs based on  $\text{ZnO}$  are not suitable for DSSCs due to the acidic nature of the typical dyes used. This could be overcome by covering a  $\text{ZnO}$ -based TCO with a thin protective Nb-doped  $\text{TiO}_2$  layer.<sup>45</sup> The challenge would be to deposit a sufficiently conductive Nb-doped  $\text{TiO}_2$  layer using scalable methods. Doping the  $\text{TiO}_2$  photoanodes with N, S, or Cr should also be employed more to improve light absorption in DSSCs. Co-doping to simultaneously improve the conductivity is also a possibility, although this would be limited by

TABLE V. Comparison of the properties of doped ZnO and TiO<sub>2</sub> used to improve charge extraction in solar cells and the corresponding improvement in device performance.

Dopant	Fabrication	Cell architecture		$J_{SC}$ (mA cm <sup>-2</sup> )	$V_{OC}$ (V)	$FF$ (%)	$PCE$ (%)	Ref.
ZnO								
In	Sol-gel	Glass/FTO/In:ZnO/	Doped ( $x = 0.01$ )	9.935	0.605	55	3.30	58
		P3HT:PCBM/MoO <sub>3</sub> /Ag	Undoped	8.392	0.613	57	2.94	
In	Microwave-assisted polyol	Glass/ITO/In:ZnO/P3HT:	With In:ZnO	7.3	0.535	54	2.3	48
		PCBM/PEDOT:PSS/Al	Without In:ZnO	5.4	0.310	24	0.4	
LiF	Solution processing	Glass/ITO/LiF:ZnO/	Doped	10.55	0.56	56	3.31	49
		P3HT:PCBM/MoO <sub>3</sub> /Ag	Undoped	9.70	0.54	56	2.94	
Nb <sup>a</sup>	Flame spray pyrolysis	Glass/ITO/PEDOT:PSS/P3HT:	Doped ( $x = 0.03$ )	13.9	0.67	...	3.62	51
		PCBM:Zn <sub>1-x</sub> Nb <sub>x</sub> O/LiF/Al	Undoped	11.5	0.65	...	2.85	
F	Chemical bath deposition	Glass/FTO/ZnO/ZnO:F or	ZnO:F	10.75	0.53	54	3.43	52
		ZnO NR/N719/I <sub>3</sub> <sup>-</sup> ,I <sup>-</sup> /Pt	ZnO NR	3.66	0.52	48	1.04	
TiO <sub>2</sub>								
F	Sol-gel	Glass/FTO/TiO <sub>2</sub> or TiO <sub>2</sub> :	Doped	19.39	0.657	64	8.07	53
		F/N3/I <sub>3</sub> <sup>-</sup> ,I <sup>-</sup> /Pt/FTO/glass <sup>b</sup>	Undoped	16.86	0.657	65	7.25	
B	Sol-gel	Glass/FTO/TiO <sub>2</sub> or	Doped (TiO <sub>2</sub> :	14.1	0.691	62.3	6.1	6
		TiO <sub>2</sub> :B/N719/I <sub>3</sub> <sup>-</sup> ,I <sup>-</sup> /Pt	boric acid = 4:1)					
			Undoped	13.0	0.696	62.1	5.6	
Zn	Sol-gel (template-assisted)	Glass/FTO/Ti <sub>1-x</sub> Zn <sub>x</sub> O <sub>2</sub> /	Doped ( $x = 0.005$ )	14.57	0.744	70	7.6	54
		N-719/I <sub>3</sub> <sup>-</sup> ,I <sup>-</sup> /Pt	Undoped	13.01	0.748	69	6.7	
Ta	Hydrothermal	Glass/FTO/TiO <sub>2</sub> /Ta:	Ta:TiO <sub>2</sub>	19.1	0.665	65	8.18	59
		TiO <sub>2</sub> /N3/I <sub>3</sub> <sup>-</sup> ,I <sup>-</sup> /Pt	TiO <sub>2</sub> only	16.4	0.715	63	7.40	
Nb	Solvothermal	Glass/FTO/Ti <sub>1-x</sub> Nb <sub>x</sub> O <sub>2</sub> /	Doped ( $x = 0.05$ )	17.67	0.70	63	7.8	56
		N719/I <sub>3</sub> <sup>-</sup> ,I <sup>-</sup> /Pt	Undoped	11.87	0.79	70	6.6	
Nb	Hydrothermal	Glass/FTO/Ti <sub>1-x</sub> Nb <sub>x</sub> O <sub>2</sub> /	Doped ( $x = 0.017$ )	14.7	0.74	72	7.9	55
		N719/I <sub>3</sub> <sup>-</sup> ,I <sup>-</sup> /Pt/FTO/glass	Undoped	14.1	0.73	70	7.1	
Nb	Sol-gel	Glass/FTO/Ti <sub>1-x</sub> Nb <sub>x</sub> O <sub>2</sub> /	Doped (20 wt.% Nb)	0.34	0.60	36	0.074	57
		MEH-PPV/Ag <sup>c</sup>	Undoped	0.12	0.78	42	0.042	

<sup>a</sup>Solar simulations were performed at a light intensity of 120 mW cm<sup>-2</sup>, rather than the standard 100 mW cm<sup>-2</sup>.

<sup>b</sup>N3 is *cis*-bis(isothiocyanato)bis(2,2'-bipyridyl-4,4'-dicarboxylato)-ruthenium(II).<sup>60</sup>

<sup>c</sup>MEH-PPV is poly[2-methoxy-5-(2-ethylhexyloxy)-1,4-phenylenevinylene].<sup>61</sup>

the complexity of the deposition method and the possibility of unintended interactions between the co-dopants, which could, for example, lead to the formation of a second phase.

Throughout this research update, we have highlighted new methods employed to dope ZnO and TiO<sub>2</sub> via scalable techniques, as opposed to the traditional vacuum-based methods (PLD, sputtering, CVD, ALD). This is important since the fundamental driving force for new generation solar cell research is the production of photovoltaics that cost less than conventional silicon-based solar cells.<sup>10</sup> Using scalable, low-cost, facile techniques is an essential component of this. Sol-gel is one of the most commonly used open-atmosphere techniques on the laboratory-scale to synthesize a variety of new doped metal oxides due to the versatile nature of this process.<sup>22,26</sup> But sol-gel is limited for large-scale production because it is a batch process with limited throughput, the precursor and product often require ageing and annealing, and the films can be porous.<sup>22</sup> Solvothermal, hydrothermal, electrodeposition, and chemical bath deposition have similar limitations, but have higher commercial potential.<sup>52,63</sup> Films can be deposited by micro-plasma oxidation over large-areas at low cost, but are limited by the high voltage (245 V) required.<sup>64</sup> Spray-pyrolysis can

also be used in a continuous process, although the precursors need to be heated to relatively high temperatures.<sup>65</sup> AALD (or spatial ALD) can be upscaled to a continuous roll-to-roll process, and has the distinct advantage of producing uniform, conformal thin films over large areas in open-atmosphere at relatively low temperatures of 120–150 °C.<sup>21,22,35</sup> However, AALD is limited by the need to have highly reactive liquid precursors for the metal oxides. These are typically expensive, pyrophoric organometallic precursors. Nonetheless, many of these precursors are the same as for conventional ALD or CVD and can be obtained commercially. Finding ways to deposit doped ZnO or TiO<sub>2</sub> using AALD, spray pyrolysis, or other solution-based processes is very worthwhile for the ultimate goal of commercialization.

ZnO and TiO<sub>2</sub> are abundant, stable materials that can be synthesized using a variety of different techniques. In new generation solar cells, they have a wide variety of applications. But each application requires different properties and doping is a cost-effective way of tailoring the properties to optimize the device performance. This includes conduction band alignment optimization, increasing the visible light absorption for DSSC photoanodes, reducing interfacial recombination when used as buffer layers, increasing conductivity and visible light transmittance when used as a TCO or to improve charge extraction from the absorber. Doping methods range from vacuum-based to open-air processing; batch processing to continuous processing. New dopants tend to be explored using vacuum-based processing and/or batch-processing techniques, such as PLD, sputtering, and sol-gel. However, even though doping is sometimes challenging using scalable techniques, it is essential to replicate these doped ZnO/TiO<sub>2</sub> materials using such approaches in order to fulfill the ultimate aim of commercializing new generation solar cells. Finally, as has been evident in this Research Update, there are often multiple dopants that can achieve the same property enhancements. If one doping system is difficult to produce using a scalable technique, it is likely that another doping system could be successfully explored instead.

The authors acknowledge the support of the Rutherford Foundation of New Zealand and the Cambridge Commonwealth Trust, Girton College Cambridge and the ERC Advanced Investigator Grant, Novox, ERC-2009-adG247276.

- <sup>1</sup> M. Graetzel, R. A. J. Janssen, D. B. Mitzi, and E. H. Sargent, *Nature (London)* **488**, 304 (2012).
- <sup>2</sup> A. J. Moulé, L. Chang, C. Thambidurai, R. Vidu, and P. Stroeve, *J. Mater. Chem.* **22**, 2351 (2012).
- <sup>3</sup> Y. S. Lee, J. Heo, S. C. Siah, J. P. Mailoa, R. E. Brandt, S. B. Kim, R. G. Gordon, and T. Buonassisi, *Energy Environ. Sci.* **6**, 2112 (2013).
- <sup>4</sup> M. Grätzel, *Nature (London)* **414**, 338 (2001).
- <sup>5</sup> A. Gadisa, Y. Liu, E. T. Samulski, and R. Lopez, *Appl. Phys. Lett.* **100**, 253903 (2012).
- <sup>6</sup> H. Tian, L. Hu, C. Zhang, S. Chen, J. Sheng, L. Mo, W. Liu, and S. Dai, *J. Mater. Chem.* **21**, 863 (2011).
- <sup>7</sup> X. Lan, J. Bai, S. Masala, S. M. Thon, Y. Ren, I. J. Kramer, S. Hoogland, A. Simchi, G. I. Koleilat, D. Paz-Soldan, Z. Ning, A. J. Labelle, J. Y. Kim, G. Jabbour, and E. H. Sargent, *Adv. Mater.* **25**, 1769 (2013).
- <sup>8</sup> S. K. Kim, W.-D. Kim, K.-M. Kim, C. S. Hwang, and J. Jeong, *Appl. Phys. Lett.* **85**, 4112 (2004).
- <sup>9</sup> Y.-J. Lee, R. J. Davis, M. T. Lloyd, P. P. Provencio, R. P. Prasankumar, and J. W. P. Hsu, *IEEE J. Sel. Top. Quantum Electron.* **16**, 1587 (2010).
- <sup>10</sup> K. P. Musselman and L. Schmidt-Mende, *Green* **1**, 7 (2011).
- <sup>11</sup> T. Gershon, *Mater. Sci. Technol.* **27**, 1357 (2011).
- <sup>12</sup> J. Tang and E. H. Sargent, *Adv. Mater.* **23**, 12 (2011).
- <sup>13</sup> L.-N. Bai, J.-S. Lian, and Q. Jiang, *Chin. Phys. Lett.* **28**, 117101 (2011).
- <sup>14</sup> B. L. Sharma and R. K. Purohit, *Semiconductor Heterojunctions* (Pergamon Press Ltd., Oxford, UK, 2011).
- <sup>15</sup> D. C. Olson, S. E. Shaheen, M. S. White, W. J. Mitchell, M. F. A. M. van Hest, R. T. Collins, and D. S. Ginley, *Adv. Funct. Mater.* **17**, 264 (2007).
- <sup>16</sup> K. Kakiage, T. Tokutome, S. Iwamoto, T. Kyomen, and M. Hanaya, *Chem. Commun.* **49**, 179 (2013).
- <sup>17</sup> X. Zhang, F. Liu, Q. Huang, G. Zhou, and Z. Wang, *J. Phys. Chem. C* **115**, 12665 (2011).
- <sup>18</sup> Z. Duan, A. Du Pasquier, Y. Lu, Y. Xu, and E. Garfunkel, *Sol. Energy Mater. Sol. Cells* **96**, 292 (2012).
- <sup>19</sup> J. Piris, N. Kopidakis, D. C. Olson, S. E. Shaheen, D. S. Ginley, and G. Rumbles, *Adv. Funct. Mater.* **17**, 3849 (2007).
- <sup>20</sup> E. Guziewicz, M. Godlewski, T. Krajewski, Ł. Wachnicki, A. Szczepanik, K. Kopalko, A. Wójcik-Głodowska, E. Przeździecka, W. Paszkowicz, E. Łusakowska, P. Kruszewski, N. Huby, G. Tallarida, and S. Ferrari, *J. Appl. Phys.* **105**, 122413 (2009).
- <sup>21</sup> P. Poedt, D. C. Cameron, E. Dickey, S. M. George, V. Kuznetsov, G. N. Parsons, F. Roozeboom, G. Sundaram, and A. Vermeer, *J. Vac. Sci. Technol. A* **30**, 010802 (2012).
- <sup>22</sup> R. L. Z. Hoye, D. Muñoz-Rojas, D. C. Iza, K. P. Musselman, and J. L. MacManus-Driscoll, *Sol. Energy Mater. Sol. Cells* **116**, 197 (2013).
- <sup>23</sup> T. Törndahl, C. Platzer-Bjorkman, J. Kessler, and M. Edoff, *Prog. Photovoltaics* **15**, 225 (2007).

- <sup>24</sup>C. Justin Raj, K. Prabakar, S. N. Karthick, K. V. Hemalatha, M.-K. Son, and H.-J. Kim, *J. Phys. Chem. C* **117**, 2600 (2013).
- <sup>25</sup>S. Iwamoto, Y. Sazanami, M. Inoue, T. Inoue, T. Hoshi, K. Shigaki, M. Kaneko, and A. Maenosono, *ChemSusChem* **1**, 401 (2008).
- <sup>26</sup>H. Liu, J. Tang, I. J. Kramer, R. Debnath, G. I. Koleilat, X. Wang, A. Fisher, R. Li, L. Brzozowski, L. Levina, and E. H. Sargent, *Adv. Mater.* **23**, 3832 (2011).
- <sup>27</sup>C. Justin Raj, S. N. Karthick, K. V. Hemalatha, M.-K. Son, H.-J. Kim, and K. Prabakar, *J. Sol-Gel Sci. Technol.* **62**, 453 (2012).
- <sup>28</sup>J. Bisquert, *ChemPhysChem* **12**, 1633 (2011).
- <sup>29</sup>S. Zhang, X. Yang, Y. Numata, and L. Han, *Energy Environ. Sci.* **6**, 1443 (2013).
- <sup>30</sup>T. Ma, M. Akiyama, E. Abe, and I. Imai, *Nano Lett.* **5**, 2543 (2005).
- <sup>31</sup>Q. Sun, J. Zhang, P. Wang, J. Zheng, X. Zhang, Y. Cui, J. Feng, and Y. Zhu, *J. Renewable Sustainable Energy* **4**, 023104 (2012).
- <sup>32</sup>C. Kim, K.-S. Kim, H. Y. Kim, and Y. S. Han, *J. Mater. Chem.* **18**, 5809 (2008).
- <sup>33</sup>T. Ikuno, R. Suzuki, K. Kitazumi, N. Takahashi, N. Kato, and K. Higuchi, *Appl. Phys. Lett.* **102**, 193901 (2013).
- <sup>34</sup>D. Muñoz-Rojas, H. Sun, D. C. Iza, J. Weickert, L. Chen, H. Wang, L. Schmidt-Mende, and J. L. MacManus-Driscoll, *Prog. Photovoltaics* **21**, 393 (2013).
- <sup>35</sup>B. Ehrler, K. P. Musselman, M. L. Böhm, F. S. F. Morgenstern, Y. Vaynzof, B. J. Walker, J. L. MacManus-Driscoll, and N. C. Greenham, *ACS Nano* **7**, 4210 (2013).
- <sup>36</sup>R. G. Gordon, *AIP Conf. Proc.* **394**, 39 (1997); P. P. Edwards, A. Porch, M. O. Jones, D. V. Morgan, and R. M. Perks, *Dalton Trans.* 2995 (2004).
- <sup>37</sup>S.-G. Ihn, K.-S. Shin, M.-J. Jin, X. Bulliard, S. Yun, Y. Suk Choi, Y. Kim, J.-H. Park, M. Sim, M. Kim, K. Cho, T. Sang Kim, D. Choi, J.-Y. Choi, W. Choi, and S.-W. Kim, *Sol. Energy Mater. Sol. Cells* **95**, 1610 (2011).
- <sup>38</sup>S.-J. Chang, J.-L. Hou, T.-J. Hsueh, K.-T. Lam, S. Li, and C.-H. Liu, *IEEE J. Photovoltaics* **3**, 991 (2013).
- <sup>39</sup>Y. Nishi, T. Miyata, and T. Minami, *Thin Solid Films* **528**, 72 (2013).
- <sup>40</sup>N. P. Dasgupta, S. Neubert, W. Lee, O. Trejo, J.-R. Lee, and F. B. Prinz, *Chem. Mater.* **22**, 4769 (2010).
- <sup>41</sup>D. Kim, I. Yun, and H. Kim, *Curr. Appl. Phys.* **10**, S459 (2010).
- <sup>42</sup>Y. C. Lin, T. Y. Chen, L. C. Wang, and S. Y. Lien, *J. Electrochem. Soc.* **159**, H599 (2012).
- <sup>43</sup>J.-H. Kim, K.-J. Lee, J.-H. Roh, S.-W. Song, J.-H. Park, I.-H. Yer, and B.-M. Moon, *J. Korean Phys. Soc.* **60**, 2025 (2012).
- <sup>44</sup>H. Kamisaka, N. Mizuguchi, and K. Yamashita, *J. Mater. Sci.* **47**, 7522 (2012).
- <sup>45</sup>J. H. Noh, H. S. Han, S. Lee, D. H. Kim, J. H. Park, S. Park, J. Y. Kim, H. S. Jung, and K. S. Hong, *J. Phys. Chem. C* **114**, 13867 (2010).
- <sup>46</sup>L. Zhao, X. Zhao, J. Liu, A. Zhang, D. Wang, and B. Wei, *J. Sol-Gel Sci. Technol.* **53**, 475 (2009).
- <sup>47</sup>T. Stubhan, H. Oh, L. Pinna, J. Krantz, I. Litzov, and C. J. Brabec, *Org. Electron.* **12**, 1539 (2011).
- <sup>48</sup>A. Puetz, T. Stubhan, M. Reinhard, O. Loesch, E. Hammarberg, S. Wolf, C. Feldmann, H. Kalt, A. Colmann, and U. Lemmer, *Sol. Energy Mater. Sol. Cells* **95**, 579 (2011).
- <sup>49</sup>J. Chang, Z. Lin, C. Zhu, C. Chi, J. Zhang, and J. Wu, *ACS Appl. Mater. Interfaces* **5**, 6687 (2013).
- <sup>50</sup>T. Minami, *MRS Bull.* **25**, 38 (2000).
- <sup>51</sup>V. Kruefu, E. Peterson, C. Khantha, C. Siriwong, S. Phanichphant, and D. L. Carroll, *Appl. Phys. Lett.* **97**, 053302 (2010).
- <sup>52</sup>L. Luo, W. Tao, X. Hu, T. Xiao, B. Heng, W. Huang, H. Wang, H. Han, Q. Jiang, J. Wang, and Y. Tang, *J. Power Sources* **196**, 10518 (2011).
- <sup>53</sup>S. Yang, S. Guo, D. Xu, H. Xue, H. Kou, J. Wang, and G. Zhu, *J. Fluorine Chem.* **150**, 78 (2013).
- <sup>54</sup>F. Huang, Q. Li, G. J. Thorogood, Y.-B. Cheng, and R. A. Caruso, *J. Mater. Chem.* **22**, 17128 (2012); K.-P. Wang, and H. Teng, *Phys. Chem. Chem. Phys.* **11**, 9489 (2009).
- <sup>55</sup>T. Nikolay, L. Larina, O. Shevaleevskiy, and B. T. Ahn, in *Proceedings of the 37th IEEE Photovoltaic Specialists Conference (PVSC)* (IEEE, 2011), p. 748.
- <sup>56</sup>X. Lü, X. Mou, J. Wu, D. Zhang, L. Zhang, F. Huang, F. Xu, and S. Huang, *Adv. Funct. Mater.* **20**, 509 (2010).
- <sup>57</sup>M. Lira-Cantu, M. Khoda Siddiki, D. Muñoz-Rojas, R. Amade, and N. I. González-Pech, *Sol. Energy Mater. Sol. Cells* **94**, 1227 (2010).
- <sup>58</sup>A. K. K. Kyaw, X. Sun, D. W. Zhao, S. T. Tan, Y. Divayana, and H. V. Demir, *IEEE J. Sel. Top. Quantum Electron.* **16**, 1700 (2010).
- <sup>59</sup>J. Liu, H. Yang, W. Tan, X. Zhou, and Y. Lin, *Electrochim. Acta* **56**, 396 (2010).
- <sup>60</sup>T. Loewenstein, K. Nonomura, T. Yoshida, E. Michaelis, D. Wöhrle, J. Rathousky, M. Wark, and D. Schlettwein, *J. Electrochem. Soc.* **153**, A699 (2006).
- <sup>61</sup>H. Yamagata, N. J. Hestand, F. C. Spano, A. Köhler, C. Scharsich, S. T. Hoffmann, and H. Bässler, *J. Chem. Phys.* **139**, 114903 (2013).
- <sup>62</sup>W. Lin, K. Ding, Z. Lin, J. Zhang, J. Huang, and F. Huang, *Cryst. Eng. Comm.* **13**, 3338 (2011).
- <sup>63</sup>J. Li, N. Lu, X. Quan, S. Chen, and H. Zhao, *Ind. Eng. Chem. Res.* **47**, 3804 (2008).
- <sup>64</sup>W. Qin, S. Lu, X. Wu, and S. Wang, *Int. J. Electrochem. Sci.* **8**, 7984 (2013).
- <sup>65</sup>X. Zhang, X. M. Li, T. L. Chen, J. M. Bian, and C. Y. Zhang, *Thin Solid Films* **492**, 248 (2005).